MÁSTERES de la UAM

Facultad de Ciencias / 16-17

Nanociencia
y Nanotecnología
Molecular
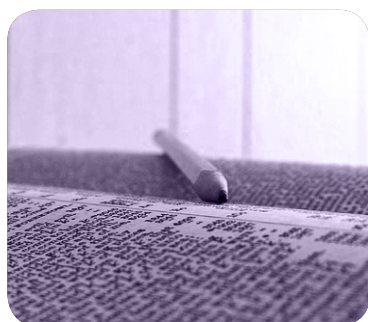
Synthesis of polyaniline and polyaniline derived carbon monoliths using eutectic solvents

Andrea Mariño López

Master in Molecular Nanoscience and Nanotechnology

Synthesis of polyaniline and polyaniline derived carbon monoliths using eutectic solvents

FACULTAD DE CIENCIAS

Andrea Mariño López

Director: Francisco del Monte Muñoz de la Peña
Codirectora: María Luisa Ferrer Pla
Tutor: Tomás Torres Cebada
Lugar de realización: Instituto de Ciencia de Materiales de Madrid (ICMM-CSIC)
Departamento de Nuevas Arquitecturas en Química de Materiales

Trabajo Fin de Máster. Curso 2016-2017

Universidad Autónoma de Madrid

Acknowledgements

Andrea Mariño López

List of abbreviations

AcGly	Glycolic acid
AHCl	Aniline hydrochloride
ChCl	Choline chloride
CV	Cyclic voltammetry
DES	Deep Eutectic Solvent
DSC	Differential scanning calorimetry
EDX	Energy-dispersive X-ray spectroscopy
EtGly	Ethylene glycol
EtOH	Ethanol
FTIR	Fourier transform infrared spectroscopy
HBA	Hydrogen bond acceptor
HBD	Hydrogen bond donor
ICP	Intrinsically conducting polymer
IL	Ionic liquid
K-L	Koutecky-Levich
LSV	Linear sweep voltammetry
NMP	1-methyl-2-pyrrolidinone
NMR	Nuclear magnetic resonance
ORR	Oxygen reduction reaction
PANI	Polyaniline
SEM	Scanning electron microscopy
T_c	Crystallization temperature
T_g	Glass transition temperature
TGA	Thermogravimetric analysis
T_m	Melting point
U	Urea
UV-vis	Ultraviolet-visible
XRD	X-ray powder diffraction

Table of contents

1. Abstract

In this work, we report the synthesis of conducting 3D free-standing PANI monoliths from aniline hydrochloride (AHCl) based deep eutectic solvents (DESs). DESs provided the monomer, the reaction and the doping media for the AHCl oxidative polymerization with ammonium persufate (APS). After washing the PANI monoliths with different acidic solutions, conductivities as high as 1 S·cm^{-1} were obtained. Moreover, conducting polymers prepared from the DES AHCl: phosphoric acid in a 1:2 molar ratio were used as precursor for the preparation of N, P-doped porous monolithic carbons after pyrolising the samples at 950 °C. The conductivity of the prepared carbons is considerable higher than those of the corresponding polymers (up to 4.95 S·cm^{-1}). A detailed characterization of the prepared DESs, conductive polymers, and their derived carbons was carried out employing different techniques, such as, ^{1}H-NMR, DSC, FTIR, UV-vis, X-ray diffraction, scanning electron microscopy, elemental and termogravimetric analysis, and conductivity measurements. The obtained N, P-doped porous carbons were found to electrocatalyse the oxygen reduction reaction (ORR) through a 2-electrons pathway.

2. Introduction

2.1 Deep Eutectic Solvents (DESs)

Deep Eutectic Solvents, a related class of ionic liquids (ILs), are mixtures of two or more components which presents a melting point lower than that of each individual component and they are generally liquid at temperatures below 100 °C.[1]

They are usually formed by complexation of quaternary ammonium or phosphonium salts, acting as a hydrogen bond acceptor (HBA), with at least one hydrogen bond donor (HBD).[2] The charge delocalization that occurs through hydrogen bonding between the halide anion and the hydrogen-donor moiety is responsible for the decrease in the melting point of the mixture relative to the melting points of the individual components.[3]

HBA (Halide salts)	HBD

Fig. 2.1 Structures of some halide salts and hydrogen bond donors used in the formation of DESs.

One of the most studied and used DES is the already commercial Reline[@], formed by choline chloride (ChCl) and urea (U) in a 1:2 molar ratio. As it can be observed in Fig 2.2, the melting point (T_m) of urea is 133 °C while that of ChCl is 302 °C. When both components are mixed in the appropriate molar ratio, the T_m can be as low as 12 °C.[3] It is important to mention that, as for ILs, it is generally understood that DESs are those mixtures that exhibit melting temperature below 100 °C, therefore, unlike ILs, where the molar ratio between the ions are fixed by the ions charge, there is a wide range of urea-ChCl compositions that are considered DES (i.e. those with molar ratios having melting points below 100 °C), increasing the possibilities of finely tuning the final DES properties (e. g. viscosity or polarity).[1]
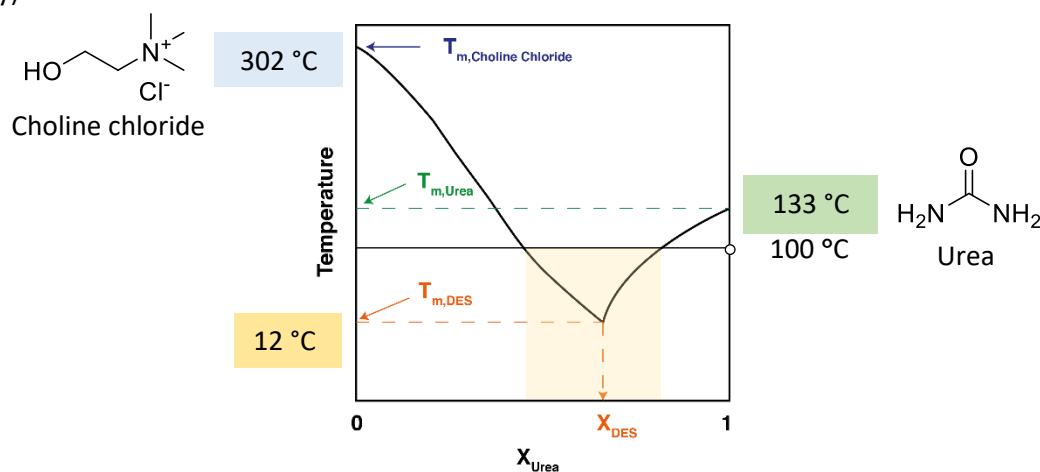
Fig. 2.2 Melting point of the different ChCl:urea mixture ratios.

DESs are similar to ILs and share many properties with them. Both, ILs and DES possess relatively high thermal and electrical conductivities, are non-reactive with water and constitute a very good reaction media for chemical reactions having excellent solvent properties. They are also non-volatile, which makes them very attractive in environmental terms as compared to conventional solvents.[2,4] While ILs purification is tedious and costly, they have been successful in many different applications ranging from gas handling, cellulose processing, solar thermal energy, and energy conversion and storage.[5,6] In these energy applications, they have been successfully tested as electrolytes in batteries, supercapacitors, actuators and in many other electrochemical devices.[7] In this context, DESs can offer additional advantages. For instance, they are easier to prepare in a purified form by just applying physical mixing of the pure components and then heating the mixture at mild temperatures (60-90 °C).[3] As suggested before, they also present wider composition versatility, and additionally, they are environmentally friendlier[1] and have lower cost than regular ILs, which makes them more desirable for large-scale applications.[2,4] It is worth mention that DES components, such as ChCl, natural carboxylic acids, amino acids, sugars, and even water, provide certain biodegradable and renewable features to the resulting eutectic mixtures.

In our group we have explored their potential as reaction media for the sustainable synthesis of different materials, such as, acrylic polymers by frontal polymerization, biodegradable polyester elastomers, and phenolic and furan resins through polycondensation reactions.[2,8] In these cases, DESs were capable of acting simultaneously as reaction media, precursor and soft template for creating hierarchical materials, and in some cases, they also acted as catalyst for the polymerization reaction.[2]

In the present work, DESs are used to carry out the synthesis of a conductive polymer, polyaniline (PANI) at high concentration. By using DESs in such a way PANI is obtained in the form of monoliths. In this case, DESs also play different roles acting at the same time as precursor, reactant system (so that solvent is not needed) and doping agent.[2] Additionally, porous doped carbons derived from PANI monoliths have been prepared and used in this work as metal free catalyst for the oxygen reduction reaction (ORR). In order to understand the properties and possible applications of the materials prepared in this work we will take a closer look at PANI and their derived carbons characterization results and then, we will correlate their physico-chemical properties with their performance in different applications.

2.2 Polyaniline (PANI) and PANI derived carbons

Conductive polymers, or more specifically, intrinsically conducting polymers (ICPs), are organic polymers that conduct electricity. Their versatility, lightweight, and processability have attracted increasing attention in different applications in many fields like, for example, electronic devices, electrocatalysis, energy storage, sensors and as doped-carbon precursor.[9,10] Among the different ICPs, polyaniline (PANI) is found to be the most intensively studied because of the advantages that it presents. It is a low cost polymer, easy to synthesize and it shows high electrical conductivity, interesting electrochemical properties and an excellent environmental and chemical stability when compared to other ICPs.[10,11]

In relation to its structure, we can find PANI in different forms, depending on its oxidation and protonation states. Taking into account the degree of oxidation, leucoemeraldine is the fully reduced form and pernigraniline the completely oxidized one. The most interesting type of PANI, also called emeraldine, is achieved when the level of reduced units are equal to the level of the oxidized ones.[11-

[13] PANI is formed by two types of units with a different structure: quinoid or benzenoid. The quinoid one is presented in the pernigraniline base, while the benzenoid ring is in the leucoemeraldine base and both of them are present in the emeraldine.[9,14]
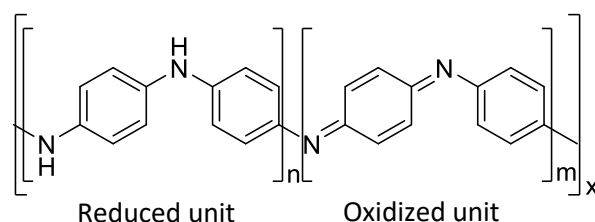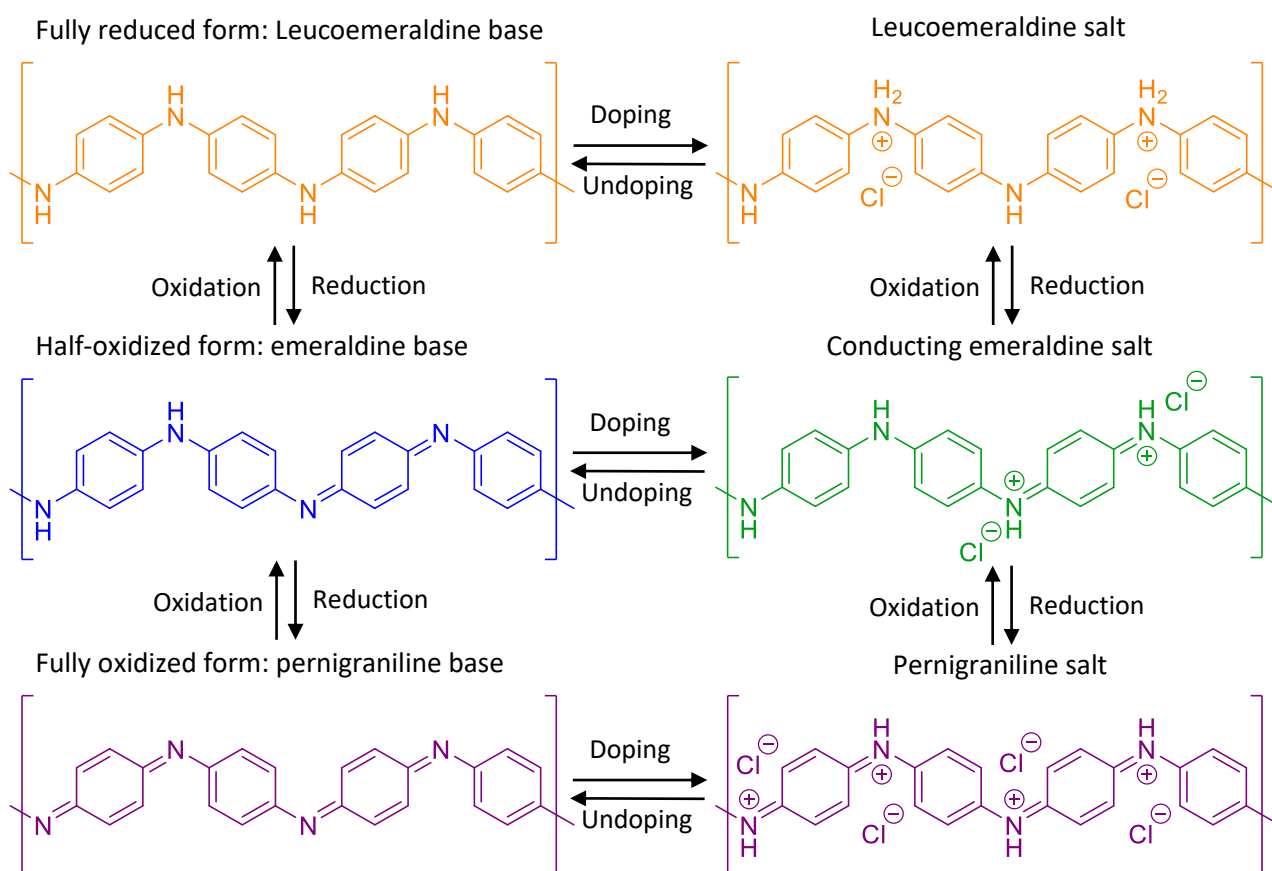

Fig. 2.3 Basic structure of PANI

Fig. 2.4 Different PANI forms.[13-15]

Both oxidized and reduced forms can be protonated in an acid media.[11] The conductive form of this polymer is the protonated one[11], while the neutral is insulating.[10] The half-oxidized and protonated emeraldine salt, which shows an intense green colour, is expected to exhibit the highest conductivity[9] (Fig. 2.4).

The regular synthesis of PANI in its doped state is carried out by using diluted aqueous solutions of aniline (ca. 0.1 M) to prevent the uncontrolled polymerization of this monomer due to autoacceleration of the reaction.[16] This fact has hindered the successful preparation of PANI monoliths. DES based synthesis of PANI allows high concentrations of the monomeric precursors in

4

the form of quaternary ammonium salt (e. g. anilinium chloride) in the reaction media. Additionally, if an acid (e. g. formic acid, glycolic acid or phosphoric acid) is chosen as HBD for DES preparation, it should be possible to obtain directly PANI in its doped state. The relatively high viscosity of DES and the monomer coordination with the corresponding H-bonding molecules should allow for a more controlled reaction and for the preparation of PANI gels and monoliths with high electrical conductivity. These materials have been very elusive and yet, only few examples of slightly conductive hydrogels have been reported using preformed hydrogels, cryogenic routes, and non-conductive gelators.[17,18]

Among the different PANI applications, its use as carbon precursor for the preparation of N-doped carbons have recently got increasing attention due to their potential use as efficient, low-cost, structurally tuneable and stable electrodes. It is now accepted that heteroatom doping into the carbon material (single and multiple element doping) can significantly improve the electrocatalytic performance of the ORR by inducing unique structural and electronic effects while maintaining strong tolerance to acidic/alkaline environment.[19] Still, different issues should be addressed before these catalysts might be ready for exploitation. For instance, uniform distribution of heteroatoms on the carbon electrocatalyst is critically important and requires a highly uniform distribution of the heteroatom in the precursors. In this context, PANI polymer will allow for a carbon precursor having a homogeneous distribution of N along the polymer chains with high N/C ratio and good stability at relatively high temperatures, which can produce high yield N-doped carbons for electrocatalytic purposes.[20] Moreover, with the versatility given by DESs based synthesis of PANI, it is possible to introduce different molecules and heteroatoms during the polymerization reaction, which can further modify and improve the performance for the ORR.[19] Finally, it is worth mention that most of these catalysts were synthesized as powders, complicating the process of electrode fabrication and also leading to the need of polymeric binders, which would lower the mass transport during the electrocatalytic process and increase the resistance of the catalytic layer. The ability to prepare free standing porous carbon electrodes from PANI monoliths would necessarily contribute to the performance of these electrodes. Since doped carbons were prepared in this work for their use in ORR and H_2O_2 production, some of the basic concepts of this reaction are discussed below.

2.3 PANI derived carbons for the electrochemical reduction of oxygen

As fossil fuels depletion approaches together with growing environmental concerns that their use implies, the development of clean and sustainable energy conversion and storage systems with high efficiency and low cost, has become now more important than ever. Electrochemical oxygen reduction is a critical process for many of these energy storage and conversion systems that operate either in acidic (for example, proton exchange membrane fuel cells) or basic electrolytes (for example, alkaline fuel cells and metal–air batteries). However, the ORR is kinetically hindered even when platinum is used as catalyst and therefore, suitable alternatives are sought in order to boost the efficiency of the process.[21]

ORR in aqueous solutions occurs mainly through two pathways: (a) the direct four-electron process where O_2 is reduced directly to H_2O and (b) the 2 electron pathway where H_2O_2 is formed (as can be seen in Table 2.1).[21,22]

Table 2.1 Electrochemical reactions and thermodynamic potentials for oxygen electroreduction.

	Acid media[21]	Alkaline media[22]
2 electron pathway	$O_2 + 2H^+ + 2e^- \rightleftarrows H_2O_2$ $E^0 = 0.69$ V $H_2O_2 + 2H^+ + 2e^- \rightleftarrows 2H_2O$ $E^0 = 1.76$ V	$O_2 + 2H_2O + 2e^- \rightleftarrows H_2O_2 + 2OH^-$ $E^0 = -0.133$ V $H_2O_2 + 2e^- \rightleftarrows 2OH^-$ $E^0 = 0.935$ V
4 electron pathway	$O_2 + 4H^+ + 4e^- \rightleftarrows 2H_2O$ $E^0 = 1.23$ V	$O_2 + 2H_2O + 4e^- \rightleftarrows 4OH^-$ $E^0 = 0.401$ V

The 2- and 4-electron reduction pathways have unique significance, depending on the applications. For instance, the 2-electron reduction pathway could be used in industry for H_2O_2 production. Hydrogen peroxide, a potential energy carrier and an environmentally friendly oxidant for various chemical industries and environmental remediation, might be produced in a more sustainable way and become an alternative to the current industrial anthraquinone based process. However, an active and cost-effective electrocatalyst which selectively reduces O_2 to H_2O_2 (2-e^- pathway) over H_2O (4-e^- pathway) is still required for this reaction.[21-24] On the other hand, in fuel cell processes, the 4-electron direct pathway is highly preferred. ORR involving 4 electrons is mostly carried out with noble metals (such as Pt and its alloys) as electrocatalysts. However, these metal-based catalysts often suffer from multiple disadvantages, such as high cost, poor stability, low selectivity, and detrimental environmental effects. This has promoted the search for cheap, stable and efficient metal-free electrocatalysts, such us the above mentioned porous N-doped carbons.[25] N-doping of carbons has already been extensively studied as it induces changes in their electronic structure (such as charge redistribution and creation of charged sites, C^+) as well as structural changes (such as high plane edge exposure), which are reported to contribute to the enhancement of kinetics of the ORR.[26,27] More recently it has been reported that by additional doping of these N-doped carbons with other heteroatoms, like B, S or P, the physical and chemical properties of carbons are further modified and new catalytic sites can be tailored.[28] As nitrogen, phosphorous is another electron donor that can provide n-type doping to the final carbonaceous structure (n-doping) and therefore, increases the carbon electron-donor properties. Moreover, studies on N-doped and N, P co-doped carbons have revealed that the additional P-doping greatly improves the catalytic activity of N-doped carbon for the ORR.[25] The preparation of DESs formed with anilinium chloride and phosphoric acid as HBD would provide a high concentration of polymer precursor in acidic media capable to incorporate N and P into the obtained porous carbon, after polymerization and pyrolysis to improve the ORR.[26]

3. Objectives

The main objective of this project was to design and evaluate a simple and sustainable route for the preparation of conductive PANI monoliths taking advantage of DES properties. After the complete characterization of these obtained 3D free standing PANI materials we also targeted the preparation of N, P co-doped monolithic carbons from these PANI monoliths and their characterization and evaluation as electrocatalysts for the ORR.

4. Materials and experimental methods

4.1 Materials

The reagents aniline hydrochloride (AHCl, ≥99.0%, Sigma-Aldrich), ethylene glycol (EtGly, ≥99.5%, 1.113 g/mL at 25 °C, Sigma-Aldrich), glycolic acid (AcGly, 99%, Sigma-Aldrich), phosphoric acid (H$_3$PO$_4$, ≥99.999%, Sigma-Aldrich), formic acid (CH$_2$O$_2$, ≥95%, 1.22 g/mL at 25 °C, Sigma-Aldrich), sulfuric acid (95.0-98.0%, 1.84 g/mL at 25 °C, Sigma-Aldrich), ammonium persulfate (APS, ≥98.0%, Sigma-Aldrich), 1-methyl-2-pyrrolidinone (NMP, anhydrous 99.5%, Sigma-Aldrich), potassium hydroxide (KOH, 90%, Sigma-Aldrich), Nafion 117 solution (~5% in a mixture of lower aliphatic alcohols and water, Sigma-Aldrich), ethanol (EtOH, 99.9%, 0.790 g/mL, Scharlau), dimethyl sulfoxide-d$_6$ (DMSO-d$_6$, 99.9%, Cambridge Isotope Laboratories, Inc.), phosphoric acid solution (85%, 1.70 g/mL at 25 °C, Fluka) and phytic acid solution (50% w/w, 1.432 g/mL at 25 °C, Sigma-Aldrich) were used as received without further purification.

4.2 Deep eutectic solvents synthesis

DESs were prepared by mixing aniline hydrochloride (2 mmol, 259.18 mg) with either glycolic acid (10 mmol, 768.18 mg), phosphoric acid (4 mmol, 392.00 mg) or with formic acid (4 mmol, 159 µL) and phosphoric acid (2 mmol, 196 mg). The mixtures were then heated at 90 °C until a homogeneous liquid was formed (approximately 10 min). On the other hand, DESs containing either ethylene glycol (10 mmol, 600 µL) or formic acid (8 mmol, 318 µL) were formed just by mixing the components and stirring using a vortex at 2500 rpm at room temperature. The resulting DES were named AGL, AP, APF, AF and AEG respectively (a summary of the prepared samples is given in Table 5.1).

4.3 Synthesis of aniline hydrochloride based deep eutectic solvents

PANI monoliths were obtained by chemical oxidative polymerization of AHCl. First, ammonium persulfate (2 mmol, 259.18 mg) was added to AHCl-based DESs in an equimolar ratio to AHCl in order to initiate the polymerization. As soon as the oxidant was added, the mixtures were vigorously stirred using a vortex at 2500 rpm, for 2 min in the case of AEG, AGL and AF DESs, and 5 min in the case of the DESs containing phosphoric acid (AP and AFP). Due to the exothermicity observed, the reaction system was placed in an ice bath for 30 min after stirring. Then, all the samples were left at room temperature for 24 h. After that, the vials containing the polymer were broken to obtain monolithic samples of PANI. These monoliths were washed with a 0.1 M acid sulphuric acid solution for 24 h. Then the samples were dried for 24 h in air and 24 h in a vacuum oven at room temperature. PANI obtained from AEG, AGL, AF, AP, and APF DESs and washed with sulphuric acid were named as PANI$_{AEG}$, PANI$_{AGL}$, PANI$_{AF}$, PANI$_{AP}$, PANI$_{AFP}$, respectively. In the case where PANI$_{AP}$ samples were subsequently washed with either 0.1 M phosphoric acid or 0.1 M phyitic acid, the resulting materials were labelled as PANI$_{AP}$-Phos and PANI$_{AP}$-Phy, respectively. Afterwards, all PANI$_{AP}$ monoliths (PANI$_{AP}$-S, PANI$_{AP}$-Phy, and PANI$_{AP}$-Phos) were pyrolyzed in a Carbolite oven at 950°C for 4 h under a nitrogen flow with a heating rate of 1 °C·min^{-1}. As a result, C-PANI$_{AP}$-S, C-PANI$_{AP}$-Phy, and C-PANI$_{AP}$-Phos carbons were obtained.

4.4 Characterization of DESs

Proton nuclear magnetic resonance (^{1}H-NMR) was performed in a Bruker spectrometer DRX 500 MHz. DESs were placed in capillary tubes, employing dimethyl sulfoxide-d$_6$ (DMSO-d$_6$) as an

external reference (the deuterium signal was used for locking and shimming the sample). ^{1}H-NMR spectra of HBD was also recorder to compare the chemical shifts of the isolated components and into the DESs. Liquid HBD were also placed in capillary tubes while solid HBD were dissolved in DMSO-d_6 to perform the spectra.

Differential scanning calorimetry (DSC) was carried out in a TA Instruments Discovery system, under a nitrogen atmosphere on an aluminium pan in a sealed furnace, and at a scan rate of 5 °C·min$^-$^{1} during the whole process. For data acquisition, the samples were cooled from room temperature to -90 °C and kept at this temperature for 10 min before starting the heating/cooling cycle, which consisted of heating the sample to 100 °C and then cooling it again to -90 °C. This cycle measurement was repeated two times and the sample was cooled to room temperature at the end of the analysis. DSC scans showed the glass transition temperature (T_g) of DESs.

4.5 Characterization of PANI polymers and PANI carbons

The morphology of the resulting monoliths was studied by scanning electron microscopy (SEM) using a Hitachi S-3000N equipment with a backscattered electron detector. The sample was placed on an aluminium stud using adhesive tape and sputter-coated with gold. EDX was also performed using this equipment.

FTIR spectra were performed in a Bruker IFS66v spectrometer in the range of 4000-600 cm^{-1} at room temperature by using KBr pellets.

X-ray Powder Diffraction (XRD) measurements were carried out using a Bruker D8 Advance Powder Diffractometre using CuKα radiation source (λ = 0.15418 nm), in a 2θ range from 5° to 70°, with step size of 0.05° and counting time of 1.5 s.

UV-visible spectra were obtained using a Variant Cary 4000 spectrophotometer. For the measurements, the samples were dispersed in N-methyl-2-pyrrolidone (NMP) with an initial concentration of 0.2 mg·mL^{-1} and placed in an ultrasonic bath for a few minutes before recording their absorption spectra.

The elemental chemical analysis of the samples was performed using a LECO Elemental Analyzer CHNS-932, where took place the full oxidation of the sample through an instantaneous combustion at 1000 °C in an oxygen-rich environment. The obtained products (CO_2, H_2O, N_2 and SO_2) were carried by Helium to individual and selective sensors, which performed fast quantitative measurements without interferences just after combustion. After that, gases were eliminated to measure N_2 by differential heat conductivity.

Thermogravimetric analyses (TGA) were performed in a temperature range between 25 °C and 1000 °C under a nitrogen flow at a heating rate of 5 °C·min^{-1} with a TGA Q600 module from TA Instruments.

BET area analysis provides the value of the surface area calculated by the Stephen Brunauer, Paul Hugh Emmett, and Edward Teller method. The information obtained from the gas adsorbed volume allows to determine the area, the porous distribution, and the size and volume of pores in the sample. An adsorption isotherm Asap2020 Micromeritics equipment was used for the measurements. N_2 was employed as adsorptive.

The electrical characterization of the samples was carried out by the determination of their electrical conductivity (σ). Resistivity is the inverse of conductivity[29] and it was calculated by using a

digital multimeter Fluke 8846A in a four-probe collinear configuration, where current was supplied through the two outer probes, while the two inner probes sensed the resulting voltage drop across the sample. The four probes were equally spaced and brought into contact with the sample. Each measurement was performed on 3 different samples and each sample was measured two times on each side.
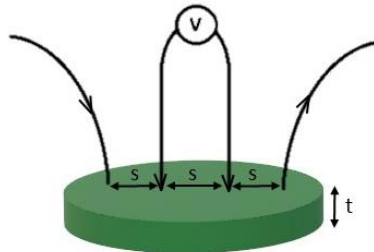
Fig. 4.1 Scheme showing the four-probe collinear configuration to measure the electrical conductivity

The resistivity (ρ) values were obtained by applying equation 4.1.

$$\rho = G \cdot \frac{V}{I} \qquad (4.1)$$

$$\sigma = \frac{1}{\rho} \qquad (4.2)$$

Where the correction factor G is a function of sample geometry, the position of the probes on the sample, and the spacing between the probes.[30] Therefore, the expressions for the factor G in the case of thin samples (pellets of 0.2-0.3 mm diameter, eq. 4.3) and thick ones (monoliths of 2-4 mm diameter, eq. 4.4) are as follows:

$$\text{Thick samples: } G = 2\pi s \cdot T_1\left(\frac{t}{s}\right) \qquad (4.3)$$

$$\text{Thin samples: } G = \frac{\pi}{ln2} \cdot t \cdot T_2\left(\frac{t}{s}\right) \qquad (4.4)$$

For thick samples, "$2\pi s$" is the geometric factor for a semi-infinite volume and $T_1\left(\frac{t}{s}\right)$ is an additional correction to apply for the finite thickness (t) of the sample ($T_1\left(\frac{t}{s}\right) \rightarrow 1$ as $t \rightarrow \infty$, and it is tabulated). For thin samples, "$\frac{\pi}{ln2} \cdot t$" is the geometric factor for an infinitely large thin slice and $T_2\left(\frac{t}{s}\right)$ is an additional correction factor to apply when t is not much less than s ($T_2\left(\frac{t}{s}\right) \rightarrow 1$ as $t/s \rightarrow 0$, and it is also tabulated).

The electrochemical catalytic activity measurements for (the study of) ORR were carried out by cyclic voltammetry (CV) and linear sweep voltammetry (LSV) on a rotating-disk electrode at a rotation rate up to 2000 rpm. A conventional three-electrode configuration consisting of a glassy carbon as working electrode, a platinum mesh as counter electrode, and a Ag/AgCl/KCl (3M) as reference electrode, was used. The electrolyte was a 0.1 M KOH solution. The carbon sample was prepared by grinding in a mortar. The obtained powder was then passed through a sieve to select a particle size between 56 and 150 μm. 5 mg of this carbon powder were added to 47.5 μL of Nafion© 117 solution and 170 μL of ethanol and sonicated for 5 min. Then a polished glassy carbon rotating-disk tip (4 mm in diameter) was coated twice by drop-casting with 3.5 μL of the slurry.[31] The electrode was thermostated at 25 °C and purged with high purity either nitrogen or oxygen for at least 30 min prior to each electrochemical measurement.

The electron transfer number per oxygen molecule (n) for ORR was determined from the LSV curves according to the Koutecky-Levich (K-L) equation, which is shown below:

$$\frac{1}{I} = \frac{1}{I_K} + \frac{1}{I_D} = \frac{1}{I_K} + \frac{1}{B \cdot \omega^{1/2}}$$

$$B = 0.620 \cdot n \cdot F \cdot A \cdot C_{O2} \cdot D_{O2}^{2/3} \cdot v^{1/6}$$

where F is the Faraday constant (F = 96485 C·mol^{-1}), C_{O2} the oxygen concentration in the solution (C_{O2} = 1.39·10-3 mol·L^{-1}), D_{O2} the diffusion coefficient of oxygen in the solution (D_{O2} = 1.9·10^{-5} cm^2·s^{-1}), v the kinematic viscosity (v = 0.01004 cm^2·s^{-1}) and ω the rotation rate.[31,32] From the slope values of the lines obtained after plotting with J^{-1} versus ω$^{-1/2}$ at each potential, the number of transferred electrons (n) can be calculated.

5. Results and discussion

5.1 DES preparation and characterization

Five different DESs were synthetized by mixing AHCl and different HBD molecules (ethylene glycol, glycolic acid, phosphoric acid, formic acid, and a mixture of both phosphoric and formic acid, see Table 5.1). For the formation of AGL, AP and APF DESs, only mild heating was applied. Unlike what is needed for regular preparation of ILs, no further purification was required.[2] The prepared DESs were used later on to synthesize PANI monoliths.

Table 5.1 Melting point of polymerizable AHCl-based DESs and their individual components.
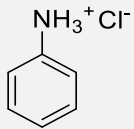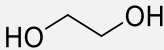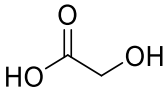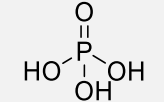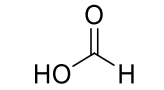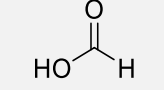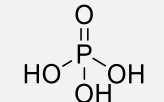
DES name	Quaternary ammonium salt	Hydrogen bond donor (HBD)	Salt:HBD (molar ratio)	Aniline hydrochloride m.p. (°C)	HBD m.p. (°C)	DES Tg (°C)
AEG		HO⌒OH	1:5	196-198	-12.9	-
AGL		HO–C(=O)–OH	1:5	196-198	75.0	-58.0
AP	NH$_3^+$ Cl$^-$	HO–P(=O)(OH)–OH	1:2	196-198	42.4	-
AF		HO–C(=O)–H	1:4	196-198	8.4	-
APF		HO–C(=O)–H ; HO–P(=O)(OH)–OH	1:2:1	196-198	-	-
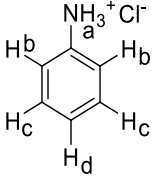
Table 5.1 shows the name, the chemical structure and the melting point of the components integrating the different DESs, their molar ratio in the mixture and the glass transition temperature of one of these DESs (no melting point was found in any case). The ratios AHCl:HBD were defined to

prepare DESs being liquid and stable at room temperature. Beside, in some cases (e. g. for AEG, AGL and AF), the ratio of HBD into the DES was increased in order to decrease the viscosity of the eutectic mixture. As mentioned before, AHCl based DES can act as *solvent designer* allowing to control the solvent properties (e. g. viscosity, polarity…) by varying the type of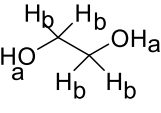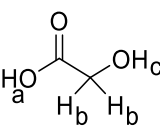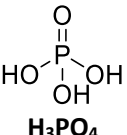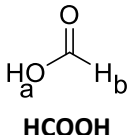 HBD, and also the salt:HBD molar ratio. The prepared DESs presented different viscosities, being higher for AP and AGL while AEG and AF presented the lowest ones. DSC analyses confirmed their eutectic nature since neither melting temperature (T_m) nor crystallization temperature (T_c) were displayed in any of the recorded DSC traces. It should be noted that this is a common feature observed for non-easily crystallisable ILs and DESs.[33] It is also worth to mention that thermal study of phosphoric based DESs could not be made because a reaction with the aluminium pan during the thermal treatment on the DSC experiments was observed.
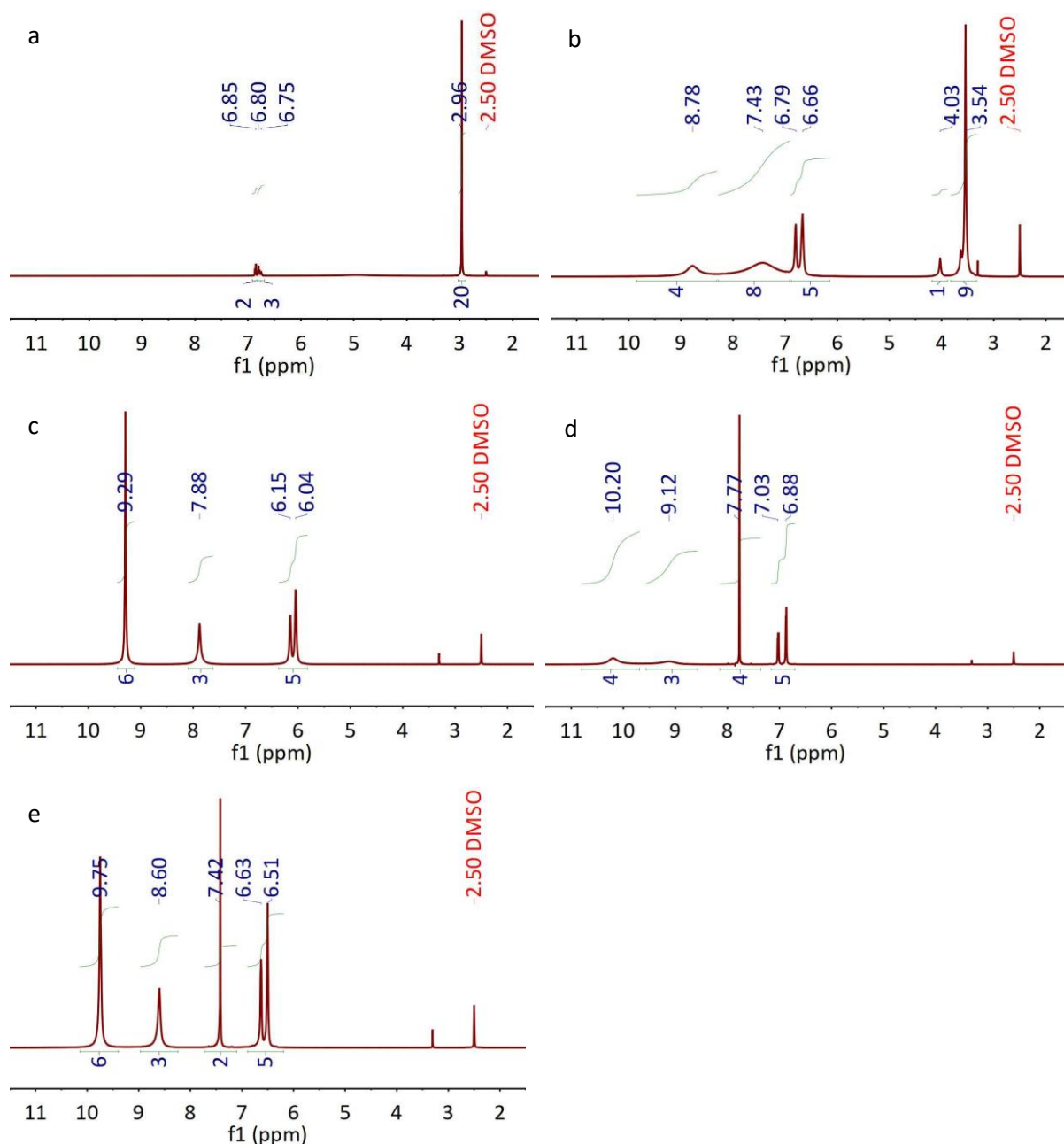
   ^{1}H NMR spectra of each DES (Table 5.2 and Fig. 5.1) allow us to verify the presence of both components in the mixture and the molar ratio between them. But what is more important, they also corroborate the formation of the different complexes by the chemical upfield shift of the signals ascribed to both components of the DESs, AHCl and the corresponding HBD, compared to those appearing in the spectra of the individual counterparts.

Table 5.2 Chemical shift of the signals ascribed to the different DESs and each individual counterpart. *Very low intensity signals.

Sample	AHCl Ha	AHCl Hc	AHCl Hb and Hd	EtGly Ha	EtGly Hb	AcGly Ha	AcGly Hc	AcGly Hb	H₃PO₄ H	HCOOH Ha	HCOOH Hb
AHCl	10.39 (3H)	7.47 (2H)	7.39 (3H)								
EtGly				4.82 (2H)	4.23 (4H)						
AcGly						12.28*	5.11*	3.9 (2H)			
H₃PO₄									-		
HCOOH										10.68 (1H)	8.37 (1H)
AEG	-	6.85 (2H)	6.78 (3H)	-	2.96 (20H)						
AGL	**	6.66 & 6.79 (5H)				**	**	3.54 & 4.03 (1H & 9H)			
AP	7.88 (3H)	6.04 & 6.15 (5H)							9.29 (6H)		
AF	9.12 (3H)	7.03 (2H)	6.88 (3H)							10.20 (4H)	7.77 (4H)
APF	9.75 (6H)	6.51 & 6.63 (5H)						Hc	8.60 (3H)	9.75 (6H)	7.42 (2H)

Fig. 5.1 NMR of the AEG (a), AGL (b), AP (c), AF (d) and APF (e) DESs.

5.2 Preparation and characterization of PANI monoliths

PANI in its conductive form was prepared using ammomium persulfate and the different DESs. As all the prepared DESs contained AHCl, they were used as precursors, as well as both, reaction and doping media for the oxidative polymerization of AHCl. Therefore, no extra solvent was needed and the polymerization was carried out in a highly concentrated media in the absence of water. A scheme of the synthesis procedure to obtain PANI monoliths from DES can be followed in Fig 5.2. The prepared

monoliths were then washed with sulfuric acid in order to remove the impurities coming from small PANI oligomers while keeping PANI its doped state.
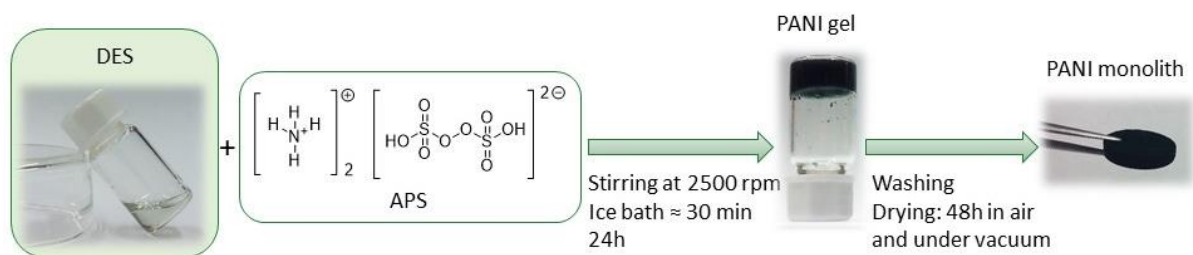
Fig. 5.2 Synthesis procedure to obtain PANI monoliths from DESs.
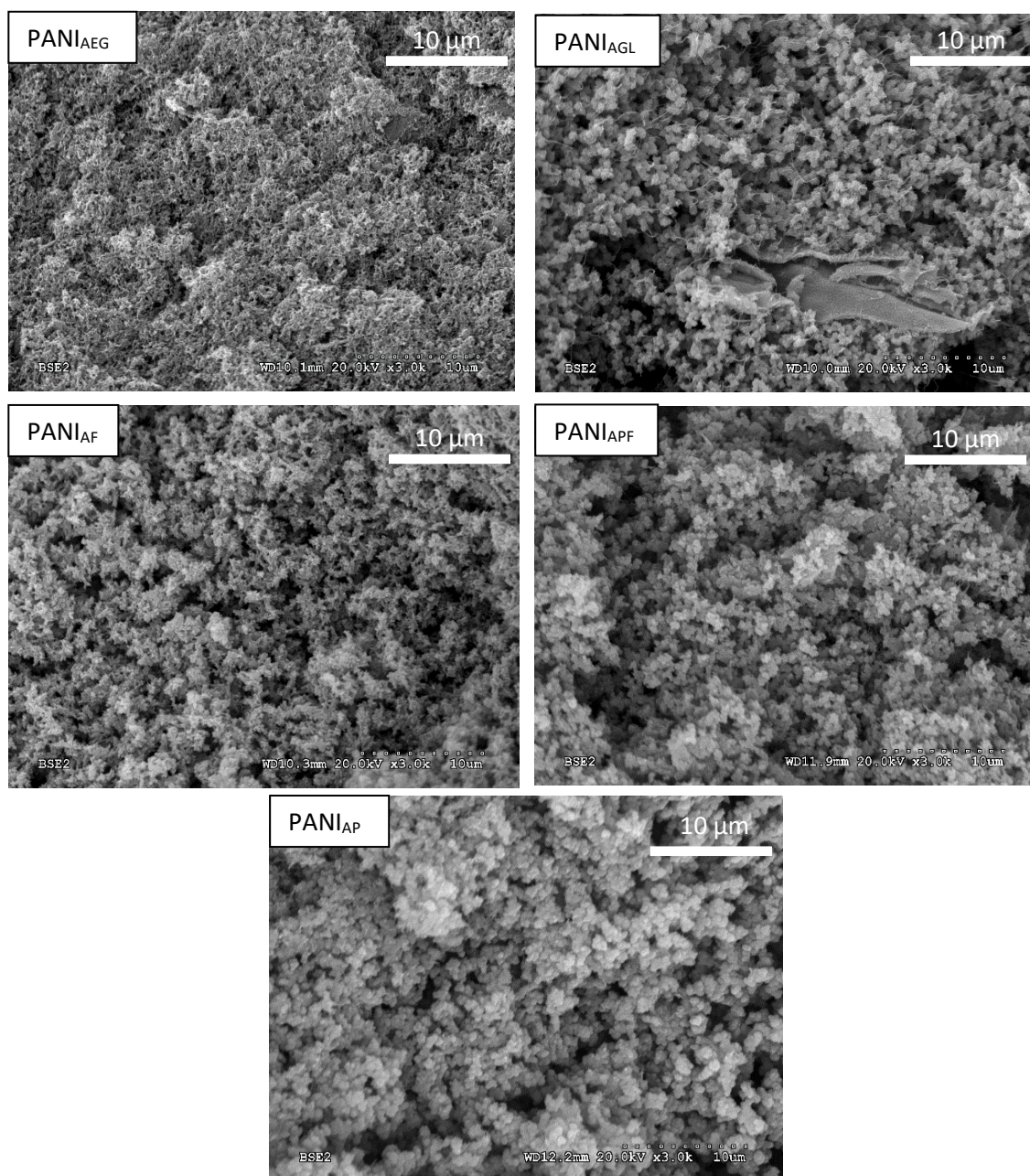
Fig. 5.3 SEM images of PANI monoliths prepared from different DESs

SEM images displayed in Fig. 5.3 show the morphology of the resulting PANI monoliths, which consisted in a porous network of globular PANI that aggregates into an interconnected structure. At low magnification (data not shown) some big pores could be observed in all samples (probably coming from bubbles formed during the mixing and polymerization process) corroborating the presence of features capable to reduce the conductivity in the PANI monoliths as compared with PANI pellets.

Some of the resulting monoliths were grounded and the obtained powder was pressed into pellets in order to obtain highly compacted material with enhanced electrical conductivities. Table 5.3 shows the conductivity of the obtained PANI monoliths and their respective pellets. The conductivity of the prepared samples indicates that all these polymers were obtained in their doped state. The highest conductivity values were observed for $PANI_{AGL}$ and $PANI_{AP}$ pellets suggesting that on the obtained monoliths, PANI chains are not as well interconnected as those in pellets submitted to pressure, impeding electron movement along the sample. Some of the prepared monoliths (i.e. $PANI_{AEG}$, $PANI_{AGL}$, $PANI_{AF}$) broke during their manipulation impeding the acquisition of the conductivity values.

Table 5.3 Electrical conductivity of PANI pellets and monoliths synthetized from different DESs.

| PANI sample	Conductivity (S/cm)	
	Monoliths	*Pellets*
$PANI_{AEG}$	-	4.33 ± 0.45
$PANI_{AGL}$	-	17.69 ± 0.88
$PANI_{AP}$	0.57 ± 0.05	10.12 ± 0.70
$PANI_{AF}$	-	0.28 ± 0.05
$PANI_{APF}$	0.25 ± 0.04	1.75 ± 0.07

In the synthesis of $PANI_{AEG}$ and $PANI_{AGL}$, the reaction takes place in liquid state at high concentration. As the polymerization proceeds, the exothermic reaction is autoacelerated and PANI is formed very quickly, making the reaction difficult to control. Moreover, as mentioned before, the mechanical properties of the obtained monoliths were rather weak impeding the conductivity measurements in the form of monoliths. $PANI_{AF}$ presented low viscosities but the same disadvantages as $PANI_{AEG}$, and $PANI_{AGL}$ with even lower conductivities. Although $PANI_{AFP}$ conductivities could be measured, the value was also low, probably due to the presence of formic acid. Therefore, further characterization was only performed on $PANI_{AP}$. In PANI samples prepared with AP DES, the polymerization occurs through a solid state reaction in a slower fashion. Moreover, phosphoric acid can serve as counter anion and the phosphate groups could be later incorporated into pyrolized samples.

Going further in the study of the PANI polymerization in solid state, it has already been stated that this process occurs through a different mechanism as compared to that in solution. As it is known, AHCl is the monomer which acts as the reductant, involving the abstraction of two electrons for the formation of a new chemical bond. On the other hand, APS is the oxidant, which accepts the two electrons and it is reduced to sulfate. Polymerization starts when both reactants are in contact. However, once some PANI has been already synthetized, electrons are easily transferred through its conductive structure and polymerization can continue without direct contact between AHCl and APS molecules.[34]
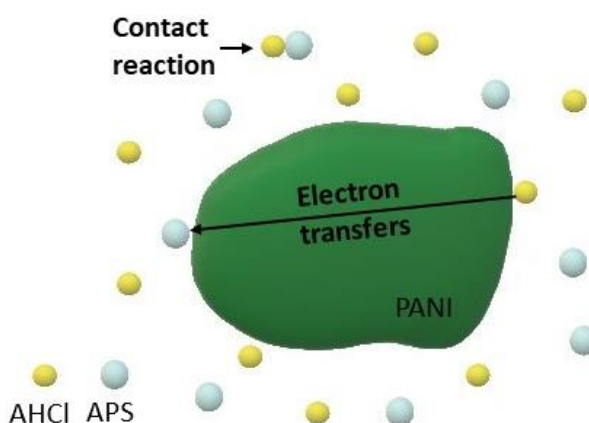
Fig. 5.4 Solid state reaction mechanism for PANI synthesis.

In order to reinforce the polymeric network and provide higher mechanical stability to the obtained monoliths, the regular washing step with sulfuric was replaced with phytic acid (Fig. 5.5). Phytic acid provides an acidic media to keep the doped state of the prepared PANI but it also can act as a crosslinker between different PANI chains due to is polyacidic character. Phytic acid is a polyphosphoric acid with six phosphoric acid groups, which electrostatically associate with protonated aniline in order to crosslink the entire network. Moreover, it has a relatively high degradation temperature ($\sim 380\,^{\circ}$ C), which prevents pore collapsing during carbonization. Thus, a fraction of the phosphoric acid groups could remain on the carbons resulting after pyrolysis conferring them catalytic properties for the ORR.[35] An additional sample was made with phosphoric acid (Fig. 5.5) washing to see any effect on changing sulfuric counter ion without the crosslinking effect. The chemical structure of the pristine PANI after the different washings were studied by FTIR, X-ray and UV-vis spectroscopies.
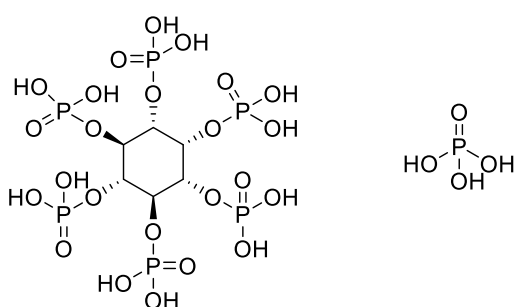

Fig. 5.5 Structure of phytic acid used as PANI crosslinker and dopant (left) and phosphoric acid used as dopant (right).
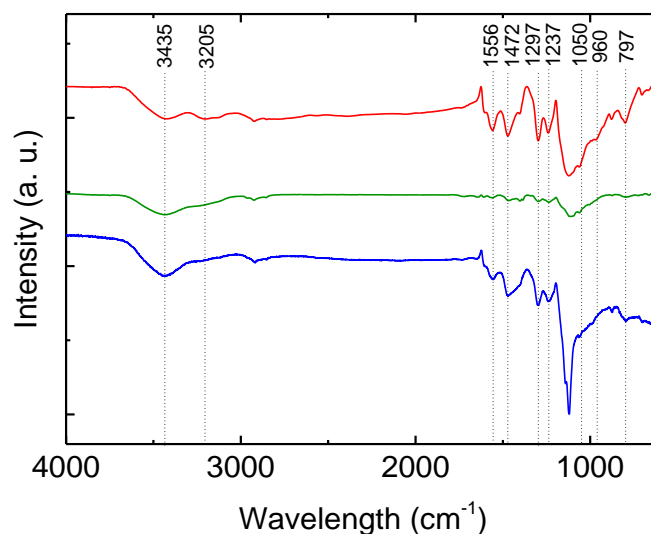
Fig. 5.6 FTIR spectra of PANI washed with different acids: PANI$_{AP}$-S (blue), PANI$_{AP}$-Phos (green), and PANI$_{AP}$-Phy (red).

FTIR spectra of the PANI$_{AP}$ monoliths washed with different acids are shown in Fig. 5.6. The broad band at 3435 cm^{-1} arises from N-H stretching vibration. The signal that appears more intense in the case of the phytic acid around 3205 cm^{-1} is assigned to the N-H$^+$, which is an indicative of doping. The bands at 1556 cm^{-1} and 1472 cm^{-1} corresponds to the C=C stretching vibration of the quinoid and benzenoid units, respectively.[13,36] The signal at 1297 cm^{-1} is ascribed to the C-N stretching of the quinoid ring and the one at 1237 cm^{-1}, which is more intense in the washed with phytic acid, corresponds to C-N$^{+\bullet}$ stretching vibration in the polaron structure.[9,36] The band at 797 cm^{-1} arises from the C-H out-of-plane bonding vibration in the 1,4-disubtituted benzene ring, that is, the para-coupled structure. The signal that appear at 960 cm^{-1} corresponds to the tetragonal PO$_4^{3-}$ vibration and that around 1050 cm^{-1} can be assigned to the phosphonic groups.[37] These characteristic bands confirm that the conducting emeraldine salt phase is present.[13,36]
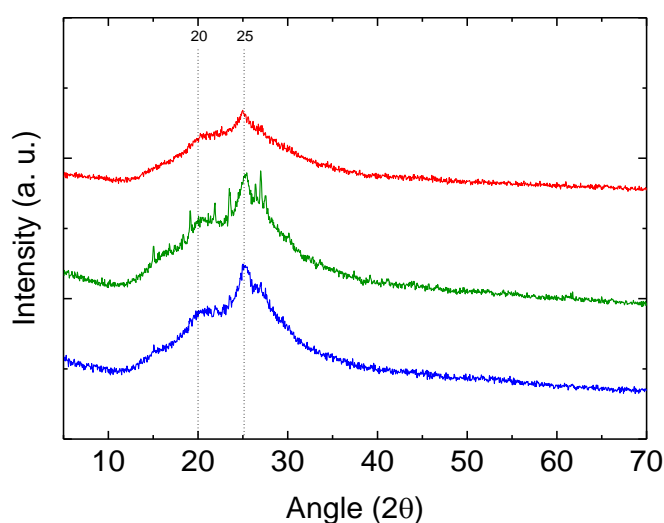
Fig. 5.7 X-ray diffraction patterns of PANI washed with different acid acids: PANI$_{AP}$-S (blue), PANI$_{AP}$-Phos (green), and PANI$_{AP}$-Phy (red).

X-ray diffraction (XRD) patterns of the three PANI$_{AP}$ samples are shown in Fig. 5.7. Very little difference is observed in them indicating that counter ion / croslinking has not great effect on the sample crystallinity. One broad band centred at 2θ = 25° and another less intense at 20° are observed. The fact that this peak is weaker than that at 25° indicates the presence of highly doped emeraldine salt and that PANI salts have some crystallinity, which can be ascribed to the repetition of quinoid and benzenoid rings along the chain. In PANI polymer, crystalline regions are conducting in nature, whereas the amorphous ones are insulating. The peak at 20° also represents the characteristic distance between the ring planes of benzene rings in adjacent chains or the close-contact interchain distance while the signal at 25° might be ascribed to the periodicity perpendicular to the polymer chain.[13,38]
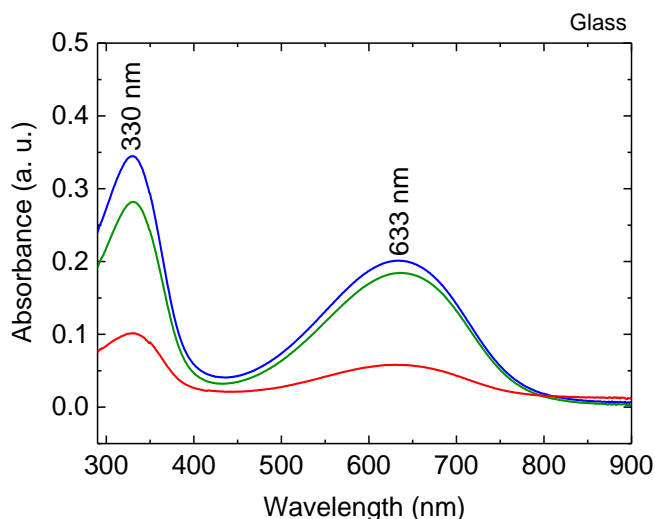
Fig. 5.8 Absorption spectra of PANI washed with different acids: PANI$_{AP}$-S (blue), PANI$_{AP}$-Phos (green), and PANI$_{AP}$-Phy (red).

Fig. 5.8 shows the UV-visible spectra of the three PANI$_{AP}$ samples disperse in NMP. Two absorption bands are observed at 330 and 630 nm. These signals are characteristic of the blue emeraldine form of PANI, because NMP provides a basic media and therefore, PANI is in its non-protonated form. The band located at 330 nm appears due to the π-π* transition of the benzenoid rings and the one at 633 nm due to the charge transfer exciton transition.[12,39]

In relation to their electrical properties, Table 5.4 shows the conductivity of the obtained PANI$_{AP}$ monoliths after different washes. From this data, phosphoric acid seems to be better dopant agent than the regularly used sulfuric acid, and also better than phytic acid. The conductivities obtained from phosphoric-DES derived monoliths are also higher than previous results for monolithic PANI-phytic hydrogels (0.11 S/cm), which also presented lower mechanical consistency. Although phytic acid acts as crosslinker in PANI monoliths and hydrogels, its inositol structure contributes to increase the insulating properties of the prepared materials.[18]

Table 5.4 Electrical conductivity of PANI washed with different acids.

PANI$_{AP}$	Monolith conductivity (S/cm)
PANI$_{AP}$-S	0.57 ± 0.08
PANI$_{AP}$-Phy	0.71 ± 0.15
PANI$_{AP}$-Phos	1.01 ± 0.10

Then TGA of the samples washed with phytic (green) and phosphoric (red) acid was carried out (Fig. 5.9) due to their higher conductivity and their capability of acting as phosphorous doping agent on the obtained carbons after a pyrolysis step.
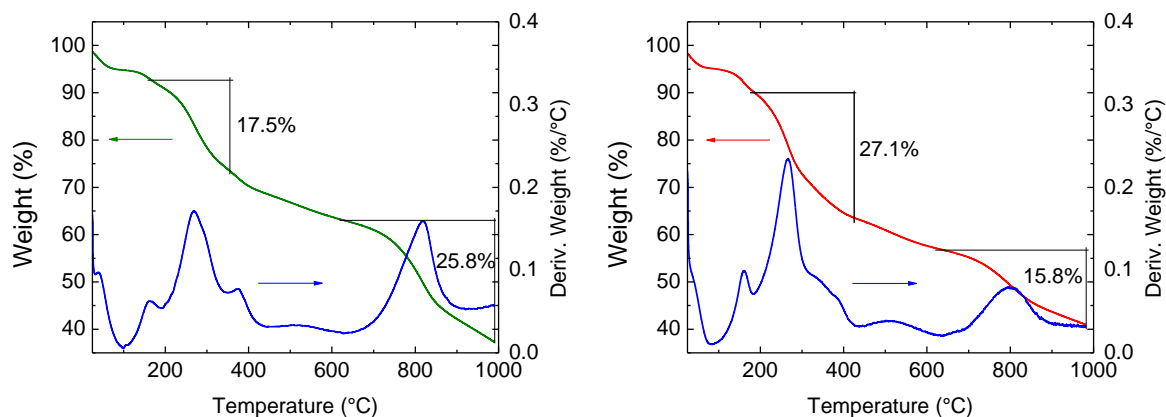

Fig. 5.9 TGA of PANI samples washed with phytic acid (left, green) and phosphoric acid (right, red).

After sample dehydration below 150 °C, TGA mainly shows two large steps of weight loss occurring during the heating of the $PANI_{AP}$ samples under a nitrogen atmosphere. However, $PANI_{AP}$-Phy suffers a higher weight loss around 800 °C, indicating better stability at lower temperatures, while in the case $PANI_{AP}$-Phos the higher decrease is around 250 °C. It has been reported that as phytic acid is carbonized, the *in situ* formed organophosphates can generate a polymeric layer through the formation of phosphonate linkages that connect and further crosslink polymer fragments helping to retain the more volatile lower molecular weight species.[35] In any case, the obtained samples render carbon yields over 40% at 950 °C and well above 50% when pyrolysed at 750 °C, which are higher than those obtained from biomass and in the order of those obtained with PANI phytic hydrogels.

5.3 Preparation and characterization of carbons monoliths

After pyrolysis at 950 °C of $PANI_{AP}$ washed in different media ($PANI_{AP}$-S, $PANI_{AP}$-Phy, and $PANI_{AP}$-Phos), the obtained carbons, C-$PANI_{AP}$-S, C-$PANI_{AP}$-Phy, and C-$PANI_{AP}$-Phos were observed in the scanning electron microscope. The achieved SEM images are shown in Fig. 5.10. It can be seen that although all samples have colloids with similar sizes, in C-$PANI_{AP}$-Phos more irregular sizes and even aggregates are also present all over the sample. This higher heterogeneity on the pyrolysed sample compared to that of $PANI_{AP}$ could indicated some structure collapse during pyrolysis causing lower conductivity than its more stable counterparts.
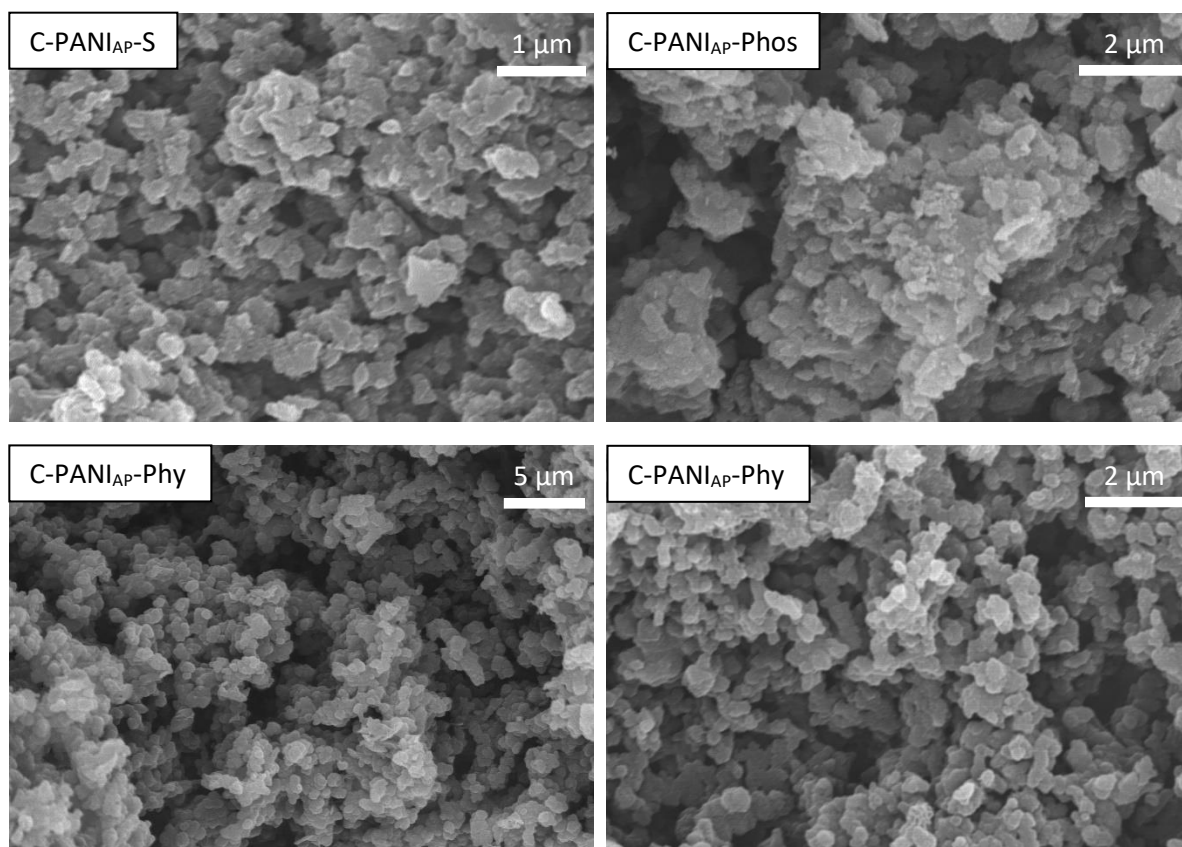
Fig. 5.10 SEM images of C-PANI$_{AP}$-S (a), C-PANI$_{AP}$-Phos (b) and C-PANI$_{AP}$-Phy (c,d) pyrolysed at 950 °C.

The conductivity of the obtained N-doped carbon monoliths was also measured and it is shown in Table 5.5. There is a remarkable increase of the conductivity in comparison to PANI$_{AP}$ monoliths values indicating than PANI monolith created a certain graphitic character that produces the increase in conductivity and maintained the monolithic structure without alterations that could lower the electrical conductivity (e. g. cracking). The lower conductivity of C-PANI$_{AP}$-Phos than its other counterparts might be due to its less stability at low temperatures during pyrolysis. In any case, all values are higher than those obtained from carbon derived from PANI-phytic hydrogels.[35]

Table 5.5 Electrical conductivity of C-PANI$_{AP}$-S, C-PANI$_{AP}$-Phos and C-PANI$_{AP}$-Phy pyrolysed at 950 °C.

Sample	Carbon monolith conductivity (S/cm)
C-PANI$_{AP}$-S	4.84 ± 0.32
C-PANI$_{AP}$-Phy	4.95 ± 0.20
C-PANI$_{AP}$-Phos	4.00 ± 0.40

The XRD patterns of the PANI carbons are shown in Fig. 5.11. As it can be seen, upon pyrolysis, the characteristic semicrystalline PANI peaks disappeared (Fig. 5.7) whilst two broad graphitic (002) and (101) diffraction peaks appeared at about 24° and 44°, respectively.[25]
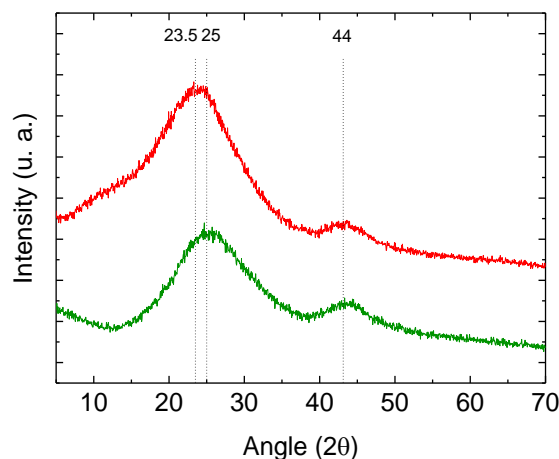
Fig. 5.11 X-ray diffraction patterns of C-PANI$_{AP}$-Phy (red) and C-PANI$_{AP}$-Phos (green) carbons pyrolysed at 950 °C.

EDX and elemental chemical analysis of the different C-PANI$_{AP}$ (obtained by pyrolysis at 950 °C of PANI$_{AP}$ after being washed using different acids) corroborate the presence of similar amounts of N in the samples (ca. 3%). Furthermore, phosphorus was found in C-PANI$_{AP}$-Phy (7.4 wt.%) and C-PANI$_{AP}$-Phos (3.2 wt.%) indicating successful co-doping of these carbons. Higher amounts of P have been observed for C-PANI$_{AP}$-Phy, which could be due to a better retention of the phosphonate groups coming from the phytic acid as crosslinker moiety at lower temperatures (as indicated by TGA curves). Additional analysis with TGA–MS is being carried out to clarify the possible P losses during the pyrolysis of the different samples. The BET surface areas of the different samples were also determined, showing slightly higher values for C-PANI$_{AP}$-Phy (338 m^2/g) than for C-PANI$_{AP}$-Phos (309 m^2/g) and, at the same time, confirming the microporous nature of both carbons. Higher surfaces areas have been observed for N, P-doped carbons derived from PANI hydrogels although in those cases samples were previously submitted to freeze-drying or further chemical activation procedures using KOH.[25,35]

5.4 Electrocatalytic oxygen reduction performance in PANI derived N, P-doped carbons.

The ORR catalytic performance of C-PANI$_{AP}$-Phy and C-PANI$_{AP}$-Phos at a constant active mass loading was first investigated by cyclic voltammetry (CV) in oxygen and nitrogen-saturated solutions of 0.1 M KOH (Fig. 5.12). Voltammograms were similar and quasi-rectangular in shape for both materials as a result of the electrochemical double layer which is formed upon ions adsorption on the pore surface of microporous carbons.[40] None of the carbons showed any obvious redox peak when the electrolyte was N$_2$-saturated. However, when the electrolyte was saturated with oxygen a cathodic peak appeared at -0.25 V for C-PANI$_{AP}$-Phy and at -0.30 V for C-PANI$_{AP}$-Phos (vs. Ag/AgCl/KCl reference electrode, see Fig. 5.12).
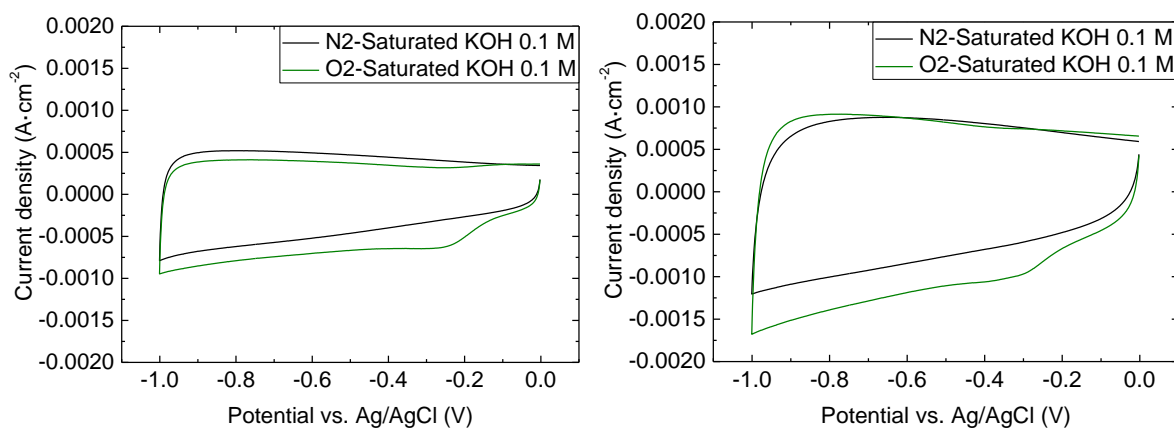
Fig. 5.12 Cyclic voltammograms of C-PANI$_{AP}$-Phy (a) and C-PANI$_{AP}$-Phos (b) in N$_2$- (black line) and O$_2$-saturated (green line) solutions.
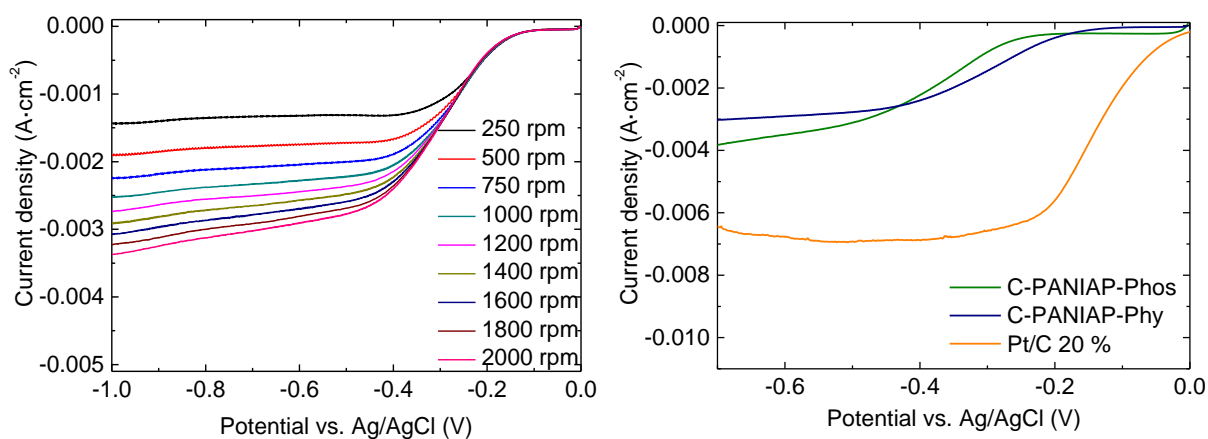

Fig. 5.13 LSV curves recorded at different rotation speeds of C-PANI$_{AP}$-Phy (a) and LSV curves recorded at 2000 rpm of C-PANI$_{AP}$-Phos, C-PANI$_{AP}$-Phy and Pt/C 20% (b) in O$_2$-saturated 0.1 M KOH.

Then, the ORR activity was further evaluated performing linear sweep voltammetry (LSV) measurements on a rotating-disk electrode at different rotating speed of up to 2000 rpm. The ORR activity is similar for both samples, although the oxygen reduction peak shifted to more positive potentials in the case of C-PANI$_{AP}$-Phy (Fig. 5.13a), probably being just a combination of higher conductivity, and slightly higher surface area. Fig. 5.13b shows LSV curves of C-PANI$_{AP}$-Phos, C-PANI$_{AP}$-Phy and Pt/C 20% at 2000 rpm. Comparing both materials with Pt/C 20%, both C-PANI$_{AP}$ showed lower ORR activities with less-positive onset potentials and lower limiting current densities. By plotting with J^{-1} versus ω$^{-1/2}$ at each potential, different lines derived from these potentials can be obtained. Both samples exhibited good linearity at values higher - 400 mV, which indicated that the current was mainly kinetically controlled.[40]
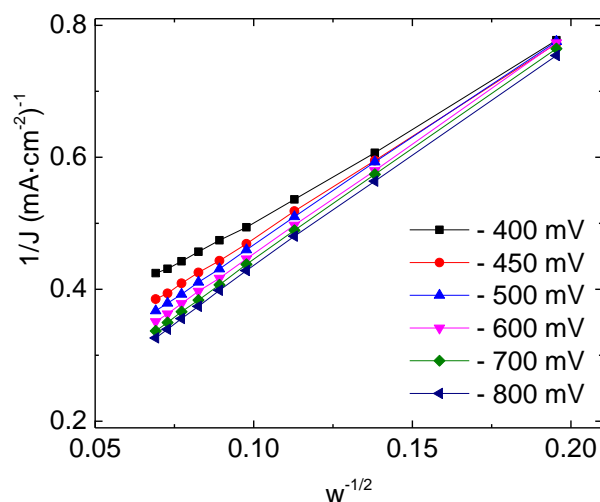
Fig. 5.14 Koutecky-Levich (K-L) lines of C-PANI$_{AP}$-Phy at different potentials.

The number of transferred electrons (n) calculated from the slope of the K-L plots for C-PANI$_{AP}$-Phos and C-PANI$_{AP}$-Phy is showed in Fig. 5.15. For comparison, "n" is also shown for a measured sample with standard Pt/C 20%, which returned values close to 4 for potentials as low as – 200 mV vs Ag/AgCl. "n" values are close to 2 for C-PANI$_{AP}$-Phos and C-PANI$_{AP}$-Phy, being the former slightly below those found for C-PANI$_{AP}$-Phy at potentials more positive than – 700 mV. The somewhat better performance of the C-PANI$_{AP}$-Phy might come from its slightly higher surface area and better conductivity. In overall, in both cases the reaction mainly occurs through the 2-electron reduction pathway. These results contrast with previous reports on PANI derived carbons, which have given values closer to 4 electrons. Moreover, P, N-doped carbons derived from samples containing PANI phytic hydrogels had shown excellent performance in ORR through a 4 electron pathway.[18,25] It should be also taken into account that in addition to the number of catalytic sites coming from the surface area and N content, the N and P species on the doped carbons (i.e pyrrolic, pyridinic, graphitic, quaternary for N and highly oxidized P and P-C binding for P) play mayor role on the ORR catalysis.[21,25] Although there is still a big controversy in regards of the contribution of each of these species of a carbon material to the ORR, further analysis using XPS is being carried out to determine the specific N and P functionalities on the surface of the carbons obtained by this DES assisted route. This will allow us to compare these results with those obtained in carbons derived from PANI phytic hydrogels.
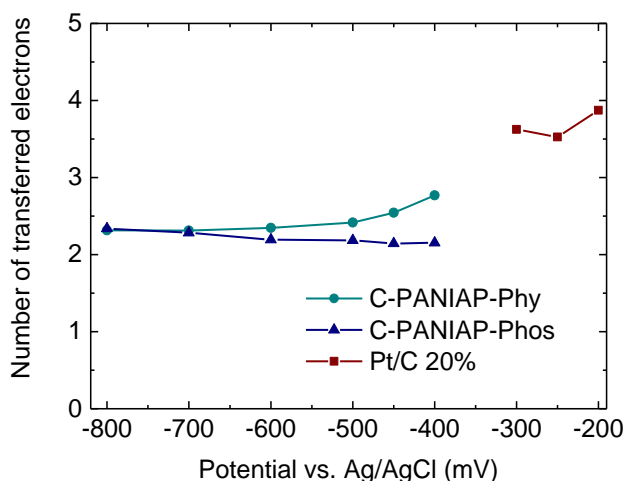
Fig. 5.15 Number of electrons transferred in each sample.

22

Finally, since C-PANI$_{AP}$-Phos and C-PANI$_{AP}$-Phy catalysts pyrolysed at 950 °C are capable to electrocatalyse the ORR through a 2-electron-transfer pathway, H$_2$O$_2$ is produced. We are currently trying to determine the selectivity of this H$_2$O$_2$ production process (which avoids to catalyse the subsequent H$_2$O$_2$ decomposition to water), specially under neutral and acidic conditions, where it has been recently claimed that N-doped carbons catalysts showed a high electrocatalytic activity, durability and selectivity toward H$_2$O$_2$ by electrochemical converting of O$_2$.[24,40]

6. Conclusions

- In this work, new AHCl-based DESs have been designed, synthesized, characterized and evaluated in a simple and sustainable route for the preparation of conductive PANI monoliths in absence of water. DES plays three important roles providing the reaction media, the doping agent, and the monomer for the AHCl oxidative polymerization. Free standing PANI monoliths in its conductive form (PANI$_{AP}$) were successfully obtained from phosphoric acid-based DESs.

- PANI monoliths were subjected to different acidic washes (either in 0.1 M phosphoric, sulphuric or phytic acid) to remove impurities and, in the case of phytic acid, to crosslink the polymer. Acidic washes of PANI monoliths (either in 0.1 M phosphoric, sulphuric or phytic acid) allow to remove impurities and, in the case of phytic acid, to crosslink the polymer in order to improve the conductivity and mechanical properties of PANI monoliths. The highest conductivity value (σ = 1 S·cm^{-1}) was achieved for PANI$_{AP}$ monolith after washing with phosphoric acid solution (PANI$_{AP}$-Phos) being one of the highest values reported for PANI in its monolithic form.

- Diverse N, P-doped carbons were obtained after pyrolysis at 950 °C of differently washed AP DES-based PANI monoliths. The conductivity of these carbons is considerably higher than that of the polymer counter parts, reaching values as high as 4.95 S·cm^{-1}.

- Complete characterization of PANI$_{AP}$ and C-PANI$_{AP}$ monoliths by different techniques (SEM, XRD, UV-VIS, FTIR, TGA, EA, EDX…) provides the knowledge of the morphology, chemical composition, and structure of these materials to better understanding the parameters that affect the synthesis in order to enhance the efficiency of the process.

- The evaluation of the electrochemical catalytic activity for ORR of different C-PANI$_{AP}$ shows a 2-electrons pathway. Further experiments are on-going to determine the selectivity of this reaction for H$_2$O$_2$ production. Additionally, XPS experiments are being conducted to determine the obtained N and P species within the C-PANI$_{AP}$ monoliths.

7. Bibliography

(1) Zhang, Q., De Oliveira, K.; Royer, S.; Jérôme, F. *Chem. Soc. Rev.* **2012**, *41*, 7108-7146.

(2) Carriazo, D.; Serrano, M. C.; Gutiérrez, M. C.; Ferrer, M. L.; del Monte, F. *Chem. Soc. Rev.* **2012**, *41*, 4996-5014.

(3) Abbott, A. P.; Boothby, D.; Capper, G.; Davies, D. L.; Rasheed, R. K. *J. A,. Chem. Soc.* **2004**, *126*, 9142-9147.

(4) Gutiérrez, M. C.; Ferrer, M. L.; Yuste, L.; Rojo, F.; del Monte, F. *Angew. Chem. Int. Ed.* **2010**, *49*, 2158-2162.

(5) Ramdin, M.; de Loos, T. W.; Vlugt, T. J. H. *Ind. Eng. Chem. Res.* **2012**, *51*, 8149-8177.

(6) Swatloski, R. P.; Spear, S. K.; Holbrey, J. D.; Rogers, R. D. *J. Am. Chem. Soc.* **2002**, *124*, 4974-4975.

(7) MacFarlane, D. R.; Tachikawa, N.; Forsyth, M.; Pringle, J.M.; Howlett, P. C.; Elliott, G. D.; Davis, J. H.; Watanabe, M.; Simon, P.; Angell, A. *Energy Environ. Sci.* **2014**, *7*, 232-250.

(8) Carriazo, D.; Serrano, M. C.; Gutiérrez, M. C.; Ferrer, M. L.; del Monte, F. *ChemSusChem* **2014**, *7*, 999-1009.

(9) Tantawy, H. R.; Aston, D. E., Smith, J. R.; Young, J. L. *ACS Appl. Mater. Interfaces* **2013**, *5*, 4648-4658.

(10) Yang, Y.; Chen, S.; Xu, L. *Macromol. Rapid Commun.* **2011**, *32*, 593-597.

(11) Santhosh, P.; Gopalan, A.; Vasudevan, T. *Spectrochim. Acta, Part A* **2003**, *59*, 1427-1439.

(12) Stejskal, J.; Kratochvíl, P.; Radhakrishnan, N. *Synth. Met.* **1993**, *61*, 225-231.

(13) Abdiryim, T.; Xiao-Gang, Z.; Jamal, R. *Mater. Chem. Phys.* **2005**, *90*, 367-372.

(14) Bhadra, S.; Kim, N. H.; Rhee, K. Y.; Lee, J. H. *Polym. Int.* **2009**, *58*, 1173-1180.

(15) Li, R. L.; Lin, C.; Shao, Y.; Chang, C. W.; Yao, F.; Kowal, M. D.; Wang, H.; Yeung, M. T.; Huang, S.; Kaner, R. B. **2016**, *8*, 401.

(16) Tzou, K.; Gragory, R. V. *Synth. Met.* **1992**, *47*, 267-277.

(17) Choi, I. Y.; Lee, J.; Ahn, H.; Lee, Ji.; Choi, H. C.; Park, M. J. *Angew. Chem., Int. Ed.* **2015**, *54*, 10497-10501.

(18) Pan, L.; Yu, G.; Zhai, D.; Lee, H. R.; Zhao, W.; Liu, N.; Wang, H.; Tee, B.; Shi, Y.; Cui, Y.; Bao, Z. *Proc. Natl. Acad. Sci. U. S. A.*, **2012**, *109*, 9287-9292.

(19) Yan, D.; Dou, S.; Tao, L.; Liu, Zhijuan; Liu, Zhigang, Hou, J.; Wang, Suangyin. *J. Mater. Chem. A.* **2016**, *4*, 13726-13730.

(20) Han, J.; Xu, G.; Ding, B.; Pan, J.; Dou, H.; MacFarlane, D. R. *J. Mater. Chem. A.* **2014**, *2*, 5352-5357.

(21) Perazzolo, V.; Durante, C.; Pilot, R.; Paduano, A.; Zheng, J.; Rizzi, G. A.; Martucci, A.; Granozzi, G.; Gennaro, A. *Carbon* **2015**, *95*, 949-963.

(22) Byers, J. C.; Güell, A. G.; Unwin, P. R. *J. Am. Chem. Soc.* **2014**, *136*, 11252-11255.

(23) Liu, Y.; Quan, X.; Fan, X.; Wang, H.; Chen, S. *Angew. Chem. Int. Ed.* **2015**, *54*, 6837-6841.

(24) Fellinger, T.; Hasché, F.; Strasser, P.; Antonietti, M. *J. Am. Chem. Soc.* **2012**, *134*, 4072-4075.

(25) Zhang, J.; Zhao, Z.; Xia, Z.; Dai, L. *Nat. Nanotechnol.* **2015**, *10*, 444-452.

(26) Wu, J.; Yang, Z.; Li, X.; Sun, Q.; Jin, C.; Strasser, P.; Yang, R. *J. Mater. Chem. A* **2013**, *1*, 9889-9896.

(27) Zhang, L.; Xia, Z. *J. Phys. Chem. C* **2011**, *115*, 11170-11176.

(28) Paraknowitsch, J. P.; Thomas, A. *Energy Environ.Sci.* **2013**, *6*, 2839-2855.

(29) Shen, L. C.; Kong, J. A. *Applied Electromagnetism*; PWS Publishing Company: Boston, **1995**.

(30) Topsoe, H. *Geometric factors in four point resistivity measurement*, 2nd ed.*;* Vadæk, **1966**; 472.

(31) Davis, R. E., Horvath, G. L., Tobias, C. W. *The solubility and Diffusion coefficient of oxygen in potassium hydroxide solutions;* Electrochimica Acta, **1967**; 12.

(32) Peng, H.; Mo, Z.; Liao, S.; Liang, H.; Yang, L.; Luo, F.; Song, H.; Zhong, Y.; Zhang, B. *Sci. Rep.* **2013**, *1756*.

(33) Gutiérrez, M. C.; Carriazo, D.; Ania, C. O.; Parra, J. B.; Ferrer, M. L.; del Monte, F. *Energy Environ. Sci.* **2011**, *4*, 3535-3544.

(34) Konyushenko, E. N.; Stejskal, J.; Trchová, M.; Blinova, N. V.; Holler, P. *Synth. Met.* **2008**, *158*, 927-933.

(35) To, J. W. F.; Chen, Z.; Yao, H.; He, J.; Kim, K.; Chou, H.; Pan, L.; Wilcox, J.; Cui, Y.; Bao, Z. *ACS Cent. Sci.* **2015**, *1*, 68-76.

(36) Konyushenko, E. N.; Reynaud, S.; Pellerin, V.; Trchová, M.; Stejskal, J.; Sapurina, I. *Polymer* **2011**, *52*, 1900-1907.

(37) Blinova, N. V.; Stejskal, J.; Trchová, M.; Prokes, J. *Polymer* **2006**, *47*, 42-48.

(38) Shao, W.; Jamal, R.; Xu, F.; Ubul, A.; Abdiryim, T. *Materials* **2012**, *5*, 1811-1825.

(39) Bláha, M.; Varga, M.; Prokes, J.; Zhigunov, A.; Vohlídal, J. *Eur. Polym. J.* **2013**, *49*, 3904-3911.

(40) López-Salas, N.; del Monte, F.; Tamayo, A.; Fierro, J. L. G.; De Lacey, A. L.; Ferrer, M. L.; Gutiérrez, M. C. *ChemSusChem* **2014**, *7*, 3347-3355.

(41) Hasché, F.; Oezaslan, M.; Strasser, P.; Fellinger, T. P. *J. Energy Chem.* **2016**, *25*, 251-257.